Contents lists available at ScienceDirect

European Journal of Pharmaceutics and Biopharmaceutics

CrossMark

Research paper

Impact of structural differences in hyperbranched polyglycerol–polyethylene glycol nanoparticles on dermal drug delivery and biocompatibility

Sumit Kumar [a,b], Nesrin Alnasif [c], Emanuel Fleige [b], Indah Kurniasih [b], Vivian Kral [c], Andrea Haase [d], Andreas Luch [d], Günther Weindl [c], Rainer Haag [b], Monika Schäfer-Korting [c], Sarah Hedtrich [c,*]

[a] Department of Chemistry, Deenbandhu Chottu Ram University of Science & Technology, Murthal (Sonepat), India
[b] Institute of Chemistry and Biochemistry, Organic Chemistry, Freie Universität Berlin, Berlin, Germany
[c] Institute of Pharmaceutical Sciences, Pharmacology and Toxicology, Freie Universität Berlin, Berlin, Germany
[d] Bundesinstitut für Risikobewertung, Safety of Consumer Products, Berlin, Germany

ARTICLE INFO

ABSTRACT

Polyglycerol scaffolds and nanoparticles emerged as prominent material for various biomedical applications including topical drug delivery. The impact of slight structural modifications on the nanoparticles' properties, drug delivery potential, and biocompatibility, however, is still not fully understood.

Hence, we explored the influence of structural modifications of five structurally related polyglycerol-based nanoparticles (PG–PEG, SK1–SK5) on dermal drug delivery efficiency and biocompatibility. The PG–PEG particles were synthesized via randomly and controlled alkylated chemo-enzymatic approaches resulting in significantly varying particle sizes and interactions with guest molecules. Furthermore, we observed considerably improved dermal drug delivery with the smallest particles SK4 and SK5 (11 nm and 14 nm) which also correlated with well-defined surface properties achieved by the controlled alkylated synthesis approach. The consistently good biocompatibility for all PG–PEG particles was mainly attributed to the neutral surface charge. No irritation potential, major cytotoxicity or genotoxicity was observed. Nevertheless, slightly better biocompatibility was again seen for the particles characterized by alkyl chain substitution in the core and not on the particle surface.

Despite the high structural similarity of the PG–PEG particles, the synthesis and the functionalization significantly influenced particle properties, biocompatibility, and most significantly the drug delivery efficiency.

© 2014 Elsevier B.V. All rights reserved.

1. Introduction

Topical drug delivery is highly interesting for local and systemic therapies. Due to the unique composition and properties of the human skin, however, the ability of substances to penetrate into or through the skin is limited and strongly depends on the physicochemical properties of the respective substance. Sufficient skin absorption is solely achieved by applying moderately lipophilic drugs ($\log P$ 1–3) with a molecular weight $\leqslant 500$ g/mol. The total cutoff for dermal absorption is 800 g/mol. Large and hydrophilic drugs including proteins and peptides are therefore nowadays excluded from topical applications. To overcome these obstacles various nanoparticulate drug delivery systems have been developed in order to improve the drug delivery into or through the skin [1–3]. Particularly hyperbranched polymers and dendrimers represent a promising opportunity [4–6] due to tailorable particle size and shape, monodispersity, and the possibility for surface modifications [7].

Despite the huge variety of dendrimers, the majority of studies have investigated two types of dendrimers for topical drug delivery: poly(amido amine) (PAMAM) and polyglycerol [7]. Aside from the above-mentioned advantages, PAMAM exhibits strong cytotoxic effects which limits its applicability [8]. A recent study described that PAMAM G2.5 shell tecto-dendrimers are tolerated well by spontaneously transformed keratinocytes (HaCaT cells) and a human colonic adenocarcinoma cell line but is still toxic for a melanoma cell line [9]. In general, the biocompatibility of

* Corresponding author. Institute for Pharmaceutical Sciences, Pharmacology and Toxicology, Freie Universität Berlin, Königin-Luise-Str. 2-4, 14195 Berlin, Germany. Tel.: +49 30 838 55065; fax: +49 30 838 53944.

E-mail address: sarah.hedtrich@fu-berlin.de (S. Hedtrich).

nanoparticulate carrier systems strongly depends on the surface charge of the particles. For example, cationic dendrimers are highly cytotoxic and hemolytic, whereas anionic [10] and PEGylated [11] particles appear to be better tolerated. Hence, dendritic polyglycerol (PG) shows high biocompatibility and is an excellent candidate for the formation of drug delivery systems due to its easy accessibility and possible variations in the degree of branching and molecular weight [12,13].

Good biocompatibility is particularly important for topical application onto diseased or barrier deficient skin. Here, the carrier system can easily come into contact with cells of the viable epidermis which particularly requires low toxicity [14]. It is still highly debated if nanoparticles are able to overcome the outermost layer of intact human skin, the stratum corneum (SC), and penetrate into deeper dermal layers. Various groups have investigated this question but obtained highly controversial results. However, evidence has emerged that nanoparticle penetration into viable layers of intact human skin is very limited [15,16]. Nevertheless, hyperbranched dendritic core–multishell (CMS) nanotransporters which are composed of a dendritic PG core surrounded by an internal C18 alkyl shell and an outermost methoxy polyethylene glycol (mPEG) shell [17] overcame the SC after a prolonged contact time of 24 h [18]. Biocompatibility studies showed no toxic effects as well as no local irritation following the topical application of CMS nanotransporters [19]. Moreover, CMS nanotransporters efficiently transport lipophilic and hydrophilic agents into the skin. For example, loading of the lipophilic model drug Nile red resulted in a 13-fold enhanced penetration into the viable epidermis [20].

Based on these promising results, we evaluated in the present study the drug delivery efficiency of five different PG–PEG nanoparticles which were composed of a dendritic PG core that was functionalized with linear PEG blocks and varying alkyl branches. We aimed to unravel the impact of the structural organization of the alkyl and PEG chains on drug loading, delivery, and biocompatibility. Therefore, we employed PG–PEG nanoparticles for skin penetration studies using the lipophilic model dye Nile red ($\log P$ 3.8, molecular weight: 318 g/mol). Additionally, we performed a comprehensive toxicity screening to assess cytotoxicity (MTT and neutral red uptake test), local irritation potential (red blood cell test, HET-CAM test), and genotoxicity (Comet assay) of the PG–PEG particles.

2. Materials and methods

2.1. Materials

PG (Mn $\cong$ 5.000 g/mol, Mw/Mn = 1.9) was prepared as previously described, using 1,1,1-tris(hydroxyl methyl)propane (TMP) as initiator [21]. Novozyme-435 was purchased from Codexis (Redwood City, CA, USA). Lewatit K1131 acidic ionic exchange resin was received from Bayer AG (Berlin, Germany). The solvent tetrahydrofuran, pyridine, methanol, and chloroform were purchased from Acros (Geel, Belgium). Dialysis was performed using Spectra/Pro membrane or benzoylated cellulose tubing (molecular weight cutoff 2000 Da), Sigma–Aldrich (Taufkirchen, Germany) changing the solvent three times over a period of 24 h. Texapon ASV 50 (INCI: sodium laureth sulfate, sodium laureth 8-sulfate, magnesium laureth sulfate, magnesium laureth 8-sulfate, sodium oleth sulfate, and magnesium oleth sulfate) was purchased from Cognis (Düsseldorf, Germany). Nile red was obtained from ABCR (Karlsruhe, Germany). Sodium dodecyl sulfate, acetone dimethyl acetal and 4-toluenesulfonic acid (PTSA), sodium hydroxide, neutral red and 3-(4,5-dimethylthiazol-2-yl)-2,5-diphenyltetrazolium bromide (MTT) and all chemicals and solvents were obtained from Sigma–Aldrich (Taufkirchen, Germany). Water of Millipore quality was used in all experiments and for the preparation of all samples.

Buffers of 0.01 and 0.10 M phosphate were prepared by weight from $Na_2HPO_4 \cdot 7H_2O$ and $NaH_2PO_4 \cdot H_2O$.

2.2. Nanoparticle synthesis, dye loading and particle characterization

Five different amphiphilic PG–PEG nanoparticles (SK1–SK5) synthesized via two different chemo-enzymatic approaches were investigated. The synthesis, characterization, solubilization, and release profile of PG–PEG nanoparticles SK1 and SK2 using Nile red as a hydrophobic drug model have been reported earlier (Fig. 1) [22]. Here, the alkyl chains were at random positions, i.e., by randomly substituting alkyl groups on terminal and hydroxyl groups of PG. A more controlled chemo-enzymatic approach was followed for the synthesis of SK3–SK5 as described in Fig. 2. Encapsulation and release of Nile red for SK5 have been studied in detail by UV–VIS, fluorescence, atomic force microscopy, and dynamic light scattering [23] (Fig. 2). For non-covalently loading, a film method was applied. Nile red was dissolved in dry tetrahydrofuran and the organic solvent was evaporated generating a thin film of Nile red. Subsequently the aqueous polymer solutions were added. Afterward, the aqueous solution was stirred for at least 18 h at room temperature. PG–PEG particles SK3 and SK4 have been reported for first time in this article. The synthesis of SK3–SK5 is a more controlled procedure, the terminal hydroxyl groups were protected first, and alkyl chains were introduced in the core. Subsequently, removal of the protection resulted in an alkyl substitution only in the core and not of the terminal functional groups. For control of the synthesized polymers, ^{1}H NMR (400 MHz) and ^{13}C NMR (100 MHz) spectra were taken at 25 °C using an ECX 400 spectrometer (Joel USA, MA, USA). The synthesis of the CMS nanotransporters and non-covalently Nile red loading (0.004%) of all nanoparticles were performed according to previously published procedures [1,17]. For a detailed description see the supplementary data.

For particle characterization, dynamic light scattering (DLS) measurements were taken using a Zetasizer Nano instrument (Malvern Instrument, United Kingdom).

2.3. Biological material

For skin penetration studies, pig skin of the axillary region from mature donor animals (breed: "Deutsche Landrasse") was provided by the Department of Comparative Medicine and Facilities of Experimental Animal Sciences, Charité (Berlin, Germany). Following the removal of subcutaneous fat, the skin was stored at −20 °C until usage.

Normal human keratinocytes (NHK) isolated from juvenile foreskin were expanded in keratinocyte growth medium (KGM BulletKit, Lonza, Cologne, Germany). Normal human dermal fibroblasts (NHDF from foreskin) and murine Balb/c 3T3 fibroblasts (Sigma–Aldrich, Taufkirchen, Germany) were cultivated in Dulbecco's Modified Eagle Medium (DMEM, Sigma–Aldrich) supplemented with 7.5% fetal calf serum, L-glutamine (5 mM), and 100 I.U./ml penicillin/100 µg/ml streptomycin (Biochrom, Berlin, Germany). Human umbilical vein endothelial cells (HUVEC) were cultivated in endothelial growth medium (EGM-2 BulletKit) purchased from Lonza.

Human blood was purchased from the German Red Cross (Berlin) and fertilized chicken eggs for the HET-CAM test were purchased from Lohmann livestock breeding (Cuxhafen, Germany).

2.4. Skin penetration studies

The efficiency of Nile red loaded PG–PEG particles for dermal drug delivery was evaluated according to validated test procedures using the Franz cell setup and full-thickness pig skin [24]. On the
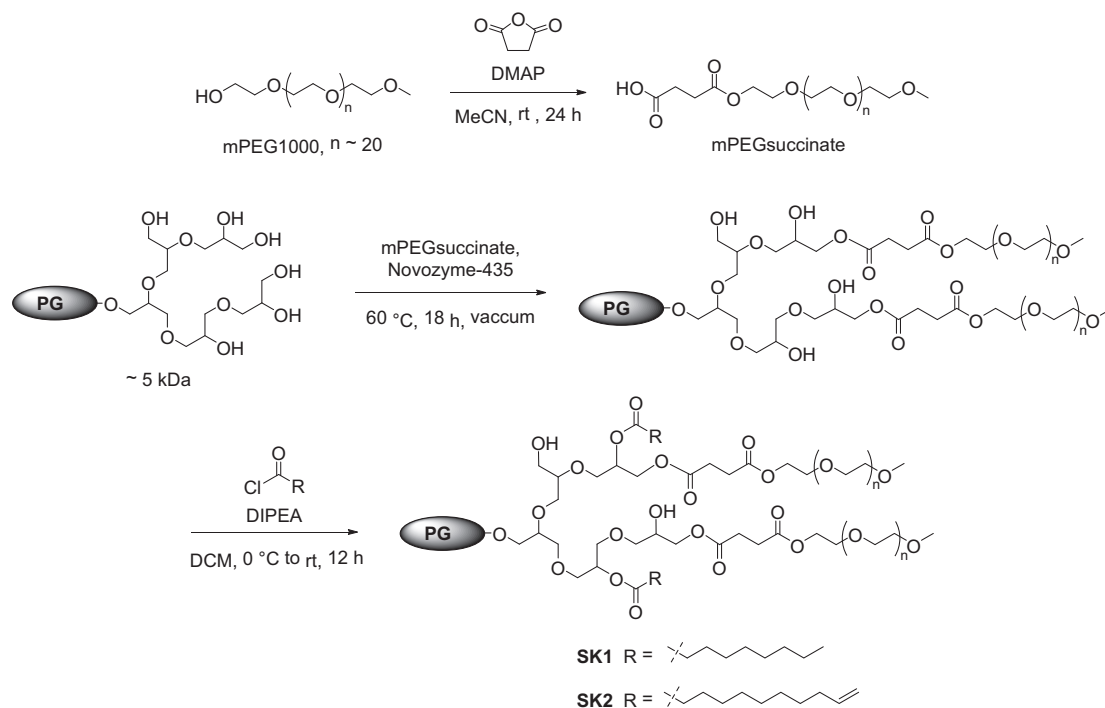
Fig. 1. 'Random' approach for the synthesis of PG–PEG based particles SK1 and SK2.
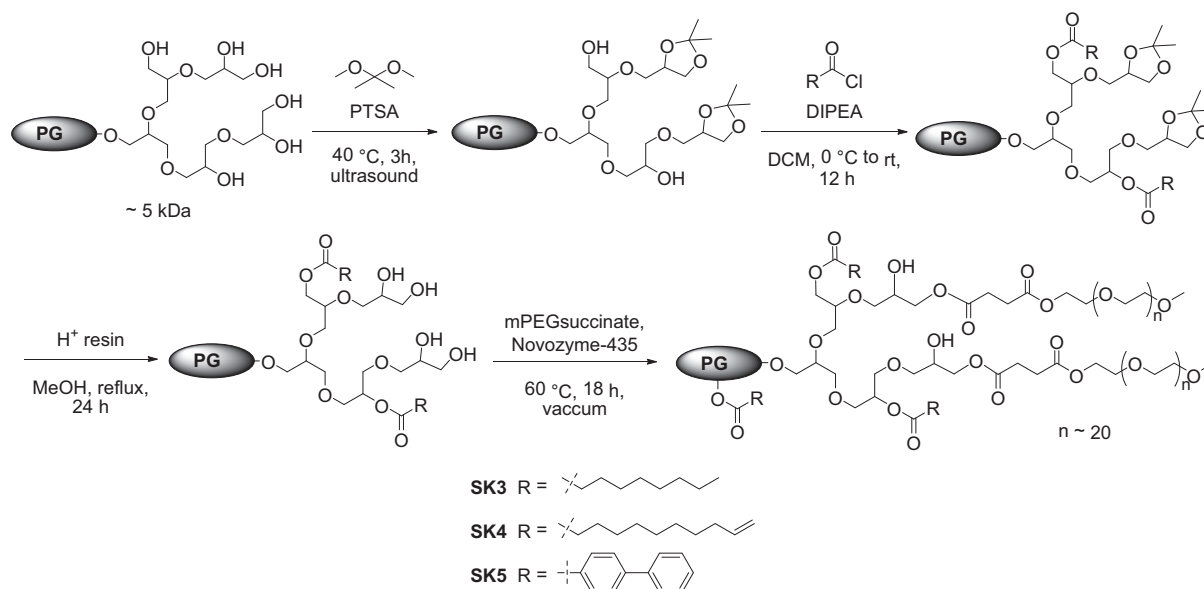
Fig. 2. 'Controlled' synthesis of the PG–PEG based particles SK3, SK4, and SK5.

day of the experiment, punched disks of pig skin (2 cm diameter) were mounted onto static-type Franz cells (diameter 15 mm, volume 12 ml, PermeGear, Bethlehem, PA, USA) with the horny layer facing the air and the dermis having contact with the receptor fluid (phosphate buffered saline (PBS) pH 7.4; skin surface temperature 32 °C). After 30 min, 20 μl/cm² of the nanoparticle formulations SK1–SK5 were applied onto the skin surface for 6 h, respectively. Subsequently, the treated skin areas were embedded in tissue freezing medium (Jung, Nussloch, Germany) and stored at −80 °C. For data analysis, 10 μm thick skin slices were prepared and subjected to normal and fluorescence light (BZ-8000 Keyence, Neu-Isenburg, Germany). The pixel brightness values (arbitrary brightness units, ABU) recorded in the viable epidermis and dermis

using an image analysis software BZ Analyser (BZ-8000 Keyence, Neu-Isenburg, Germany) gave the relative dye content in the regions of interest and were used to semi-quantify the amount of Nile red [19].

2.5. Cytotoxicity and phototoxicity

To determine potential cytotoxic effects of the SK1–SK5, the activity of the cellular mitochondrial dehydrogenase was determined by MTT reduction assay. NHK, HUVECS and NHDF (10⁴ cells per well) were seeded into 96-well plates (TPP, Trasadingen, Germany). After 24 h, PG–PEG particles SK1–SK5 (0.05% and 0.005%) were added for 24 and 48 h, respectively. Subsequently,

the cells were incubated with 10 µl MTT solution (5 mg/ml in PBS) for 4 h. After removing the supernatants, 50 µl dimethyl sulfoxide was added to dissolve the formazan salt and its optical density (OD) was measured using a microplate reader setting the excitation to 540 nm. 0.01% SDS served as the positive control. Untreated cells served for reference, the measured absorbance values were set 100%. A cell viability $\leqslant 80\%$ predicts cytotoxic effects. In a second approach, the neutral red uptake test was performed. Briefly, NHK, NHDF, and HUVEC were seeded at a density of 1.0×10^4 cells per well 96-well plates and incubated with SK1–SK5 at different concentrations (0.05% and 0.005%) for 24 h and 48 h at 37 °C, 5% CO_2, respectively. Subsequently, 100 µL of DMEM medium containing neutral red (4 mg/mL) was added. After 3 h, 150 µL of the dye release agent (1% acetic acid, 50% ethanol, 49% water) was added and the OD was analyzed using a microplate reader setting the excitation to 540 nm [25,26].

The 3T3 neutral red uptake (NRU) phototoxicity test was performed according to the INVITTOX Protocol No. 78 [27,28]. 3T3 Balb/c fibroblasts (10^4 cells per well) were seeded into 96-well plates. After 24 h, PG–PEG particles SK1, SK4 and SK5 were added using increasing concentrations (4.68–993.83 µg/ml). Chlorpromazine solutions (0.22–46.51 µg/ml) served as positive control. After incubation for 60 min, one plate was exposed to UVA for 50 min (5 J/cm^2; 1.7 mW/cm^2, solar simulator SOL500, Dr. Hoenle UV Technology, Munich, Germany) whereas the other plate was kept in the dark. Subsequently, the cells were washed twice, re-incubated with culture medium overnight and subsequently the cell viability was assessed using the NRU assay. Based on the IC_{50} (µg/ml) in the presence and absence of UVA exposure, the photo irritation factor (PIF) and mean photo effect (MPE) were calculated using phototox software (3T3 NRU PT Phototox Version 2.0) [29,30]. Phototoxicity is classified according to PIF and MPE: non phototoxic (PIF < 2 or MPE < 0.1), probably phototoxic (2 < PIF < 5 or 0.1 < MPE < 0.15) or phototoxic (PIF > 5 or MPE > 0.15).

2.6. Irritation potential

The irritant potential of the PG–PEG particles SK1, SK4 and SK5 was studied employing the hen's egg test chorioallantoic membrane (HET-CAM) test which is predictive for acute irritation potential in the eyes [31]. The eggs were kept in an incubator with automatic rotation device (Bruja, Hammelburg, Germany) at 37.5 °C for nine days. The fertilized eggs were opened and the visible white egg membrane was removed. Subsequently, PG–PEG SK1, SK4 and SK5 particles (300 µl) were applied onto the underlying chorioallantoic membrane (CAM) which was then monitored using a stereomicroscope equipped with a camera (Olympus, Tokyo, Japan). For documentation, pictures of the untreated and treated CAM were taken. For data analysis the reaction time method was used. During the residence time of 5 min, the CAM was monitored for the occurrence of hemorrhage, intravascular coagulation, extravascular coagulation, and vessel lysis using six eggs, respectively, which then were classified as none, weak, moderate, or severe reaction. For a semi-quantitative evaluation of the reactions, the reference substances Texapon ASV (0.5%, 1%, 5%), sodium hydroxide (0.2%, 0.3%, 0.5%) and acetic acid (0.3%, 3%, 30%) were applied onto two eggs, respectively (data not shown).

For data verification, the red blood cell (RBC) test was performed according to validated protocols [32,33]. Human erythrocytes separated from fresh human blood (four donors) were adjusted to 5×10^9 cells per ml by centrifugation and 25 µl of the erythrocyte suspension was added to 975 µl nanoparticle dispersions (0.005%, 0.5%). Double distilled water served as positive control, PBS for negative control and SDS solutions (0.001–0.008%) for reference. After 10 min, the suspensions were centrifuged at 10,000 rpm for 1 min and the hemolysis (%) was

determined by measuring the absorbance of the released oxyhemoglobin at 560 nm using UV/Vis spectroscopy (WPA Biowave, Biochrom, Cambridge, UK). For further data evaluation, hemolysis (H%) was plotted against the concentration of nanoparticle dispersions and the control solutions.

2.7. Genotoxicity assay

To detect DNA damage in NHK and NHDF caused by the nanoparticles SK1, SK4, and SK5, single-cell gel electrophoresis was performed (Comet assay [34]). The cells were cultivated in 24-well plates (14,000 cells/well) for 24 h and subsequently exposed to PG–PEG SK1, SK4 and SK5 (0.005% and 0.05%) for 24 h and 72 h, respectively. Afterward, cells were embedded in low melting-point agarose (0.5% in PBS) at 37 °C, transferred to a glass microscope slide which was pre-coated with normal melting-point agarose (1% in PBS), and kept for 5 min at 4 °C. The slides were immersed in a cold lysing solution of 10% DMSO, 89.9% lyse buffer (2.5 M NaCl, 100 mM Na_2EDTA, 10 mM Tris, pH 10) and 0.1% Triton X-100 overnight at 4 °C. Subsequently, the slides were incubated with electrophoresis buffer for 20 min and electrophorized for 30 min at 39 V and 450 mA (electrophoresis chamber Carl Roth, Karlsruhe, Germany). Following fixation, the slides were dried and stored until ethidium bromide (10 µg/ml) staining. The tail moment was calculated for 50 cells per slide (total of 200 cells per treatment) using the Comet Image Analysis system (CometImager Software, MetaSystems, Germany) connected to a fluorescence microscope (Zeiss, AxioVert, 400× magnification, excitation filter 515–560 nm, barrier filter 590 nm). Untreated cells were studied for baseline comet formation and 5 µM methyl methane sulfonate (MMS, 2 h) served as positive control.

2.8. Statistical analysis

Statistical analysis was conducted using GraphPad Prism, version 5.03 (San Diego, California). When comparing three or more conditions, a one-way analysis of variance (ANOVA) with a Bonferroni post hoc test was performed. $p \leqslant 0.05$ indicates statistically significant differences. The data are presented as the mean value ± standard deviation (SD) calculated from three to four independent experiments.

3. Results and discussion

Hyperbranched and dendritic nanoparticles possess favorable properties and allow for improved bioavailability as well as controlled drug release and targeted delivery. Due to the highly biocompatible nature of dendritic PGs, these polymeric structures are of utmost interest for the diagnosis and treatment of various diseases [22]. Additionally, dendritic nanoparticles are highly interesting for a local therapy of skin diseases. Previous studies from our lab demonstrated the superiority of dendritic CMS nanotransporters over lipidic carrier systems and conventional cream formulations in terms of topical delivery of hydrophilic and lipophilic compounds [19,20]. However, the mechanism of the improved drug transport is still ambiguous.

In the present study, we compared the efficiency of five different PG–PEG particles with CMS nanotransporters in terms of dermal drug delivery. Additionally, we studied the toxicity and biocompatibility of non-loaded PG–PEG particles employing different *in vitro* setups. Knowledge about the toxicity of locally applied carrier systems is of great importance, particularly in diseased or barrier impaired skin, because the nanoparticles can penetrate into deeper dermal layers and be taken up into the systemic circulation [14,18]. In contrast to CMS nanotransporters, PG–PEG particles are

less structurally defined and the alkyl and PEG chains are randomly attached to the dendritic PG core without a multishell formation [22].

PG–PEG carrier systems may represent a new and promising system for drug delivery [12,22]. The particles SK1, SK2 [22], and SK5 [23] have been reported previously. We describe here for the first time the synthesis and characterization of SK3 and SK4. A comprehensive study, however, on the efficiency of these particles in terms of topical drug delivery and a systematic assessment of biocompatibility was still missing. By studying the effects of PG–PEG carriers on skin penetration, we also aimed for a better understanding of the delivery mode of hyperbranched carrier systems.

3.1. Synthesis and PG–PEG particle characterization

The polyfunctional polyol architecture of hyperbranched PG makes them a suitable candidate for multiple functionalizations. The presence of primary and secondary alcoholic groups provides a platform for the selective modification and tuning of the physiochemical properties. The five PG–PEG nanoparticles of interest have a similar structure but differ considerably when taking a closer look. The particles consist of a functionalized hyperbranched PG core that is attached to linear PEG blocks and alkyl chains. SK1 and SK2 were synthesized via a strategy where alkyl chains are at random positions on terminal and core hydroxyl groups of the PG. Due to the randomness of the alkyl groups, SK1 and SK2 nanoparticles are bigger as they have alkyl chains on the outside and therefore form aggregates upon hydrophobic interactions between the alkyl chains resulting in aggregates of 125–175 nm (Table 1). For SK3–SK5 a different synthesis strategy was followed: Initially, the terminal hydroxyl groups on the surface of the PG were protected using acetone dimethyl acetal. Afterward, different alkyl chains were introduced to the PG core by using the corresponding carboxylic acid chlorides (Fig. 2). Subsequently, the protection was removed using acidic ion exchange resin resulting in an alkyl substitution only in the core and not on the surface of the PG. Finally, the primary hydroxyl groups on the surface were reacted with mPEG succinate using a chemo-enzymatic approach. Hence, these particles solely exhibit hydrophobic alkyl substitution in the core and not in terminal regions resulting in more defined architectures and more precise amphiphiles. Additionally, PEG is shielding these alkylated areas so that the single particles cannot aggregate upon hydrophobic interactions and therefore exist as single particles at least in the unloaded state (Table 1). However, when loading Nile red, the formation of larger aggregates (100–200 nm) was observed which is most likely initiated by hydrophobic interactions between Nile red molecules which tends to be located in the outer shell of the particles [23]. The structure of the particles as well as the degree of functionalization with the hydrophobic side chains and the mPEG shells was determined by NMR spectroscopy. The functionalization of all particles with the hydrophobic chains as well as with the mPEG was found to be 50%. In general, the PDI of all formulations was in the same and for polymeric particles in the typical range, no major differences were detected.

Table 1
Particle size and polydispersity index (PDI) of unloaded PG–PEG particles SK1–SK5.

PG–PEG	Polymer concentration (mg/ml)	Average diameter (nm)	PDI
SK1	1.0	125	0.221
SK2	1.0	175	0.228
SK3	1.0	25	0.231
SK4	1.0	14	0.308
SK5	1.0	11	0.285

3.2. Dermal drug delivery

In order to elucidate the potential of the five PG–PEGs for topical drug delivery, skin penetration studies were performed. For comparison, we also included CMS nanotransporter in the testing. The skin penetration studies were performed in pig skin which is an accepted alternative for human skin due to the limited availability of human skin [24,35]. The representative fluorescence images of skin sections after 6 h exposure to PG–PEG particles and CMS nanotransporters shown in Fig. 3A demonstrate that particularly SK4 and SK5 efficiently transport Nile red into the viable epidermis and dermis. In contrast, the larger particles SK1–SK3 were less efficient and mainly resulted in dye accumulation in the SC. These observations were supported by an evaluation of the arbitrary pixel brightness units (Fig. 3B).

All tested formulations exhibited amphiphilic properties most likely advocating intensive interactions with the skin surface and, hence, facilitating the drug transport into the skin. In contrast to CMS nanotransporters, PG–PEG particles did not form core–shell structures but had a homogeneous distribution of alkyl and PEG chains attached to the PG core. It was assumed for CMS nanotransporters that lipophilic compounds such as Nile red were mainly located in the inner shell, the alkyl chains, due to lipophilic–lipophilic interactions. A recent study on the thermodynamic behavior of Nile red after loading onto CMS nanotransporters clearly showed that in a polar environment such as water, Nile red molecules were located in the alkyl shell of the nanotransporters. A less polar environment and temperatures $\geqslant 31$ °C shifted the hydrophobic cargo toward the outermost shell; a more hydrophilic mPEG favored the release upon interaction with target structures [36]. The skin surface temperature is about 32 °C which nicely fit with the phase transition temperature of the CMS nanotransporters.

In PG–PEG particles, Nile red is mainly located in the terminal part of the hyperbranched PG, too [23]. Nevertheless, PG–PEG particles differed in terms of their topical drug delivery efficiency. Possible explanations for the superiority of SK4 and SK5 are their more hydrophobic character compared to SK1–SK3 (Figs. 1 and 2) due to the C9 chain in SK4 and the ring substitutes in SK5, intensive interactions with Nile red due to pi–pi interactions, and the smaller particle size (SK4 14 nm; SK5 11 nm) compared to SK1, SK2, and SK3 (125 nm, 175 nm, and 25 nm, respectively). Accordingly, there is some evidence that smaller nanoparticles deliver agents more efficiently into the skin compared to larger particles [37].

In spite of the growing knowledge about interactions between nanoparticles and the skin, the exact mechanism how (polymeric) nanoparticles enhance topical drug delivery is still being discussed. One possibility is that the particles themselves overcome the SC and co-transport the loaded compounds into deeper dermal layers. However, recent studies of our group clearly showed that after 6 h CMS nanotransporters did not penetrate into viable skin layers but accumulated in the SC [18]. In general, the magnitude of skin absorption of nanoparticles is still the subject of ongoing research with often contradictory results. Some nanoparticles are able to overcome the intact SC and reach the viable epidermis, whereas others obviously fail to access the viable skin [38–40]. Particles with sizes $\leqslant 30$ nm might penetrate into deeper skin layers via the intercellular route [41], although controversial results have been published [39]. With respect to PG–PEG nanoparticles, we did not expect them to overcome the SC within 6 h because of their similarity with CMS nanotransporters and their high molecular weight (approx. 60,000 Da).

Another potential mechanism is that dendrimers act as a drug release modifier [7]: Lipophilic compounds such as Nile red have been solubilized and encapsulated in the dendritic particles. Hence, the penetration limiting step is the drug release from the
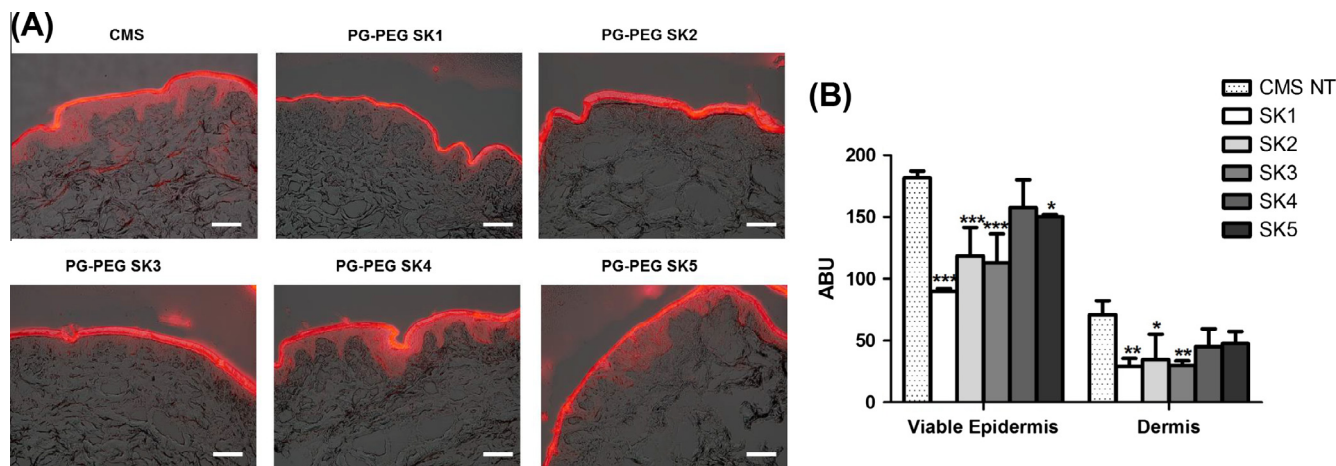
Fig. 3. Skin penetration of Nile red loaded onto PG–PEGs (SK1 ▢, SK2 ▢, SK3 ▢, SK4 ▢, SK5 ▪), and CMS-NT (▫) into pig skin. (A) representative overlay images (fluorescence and bright field; scale bar: 50 μm) of the same area, (B) Semi-quantitative data evaluation of fluorescence intensities in the viable epidermis and dermis depicted as arbitrary pixel brightness units (ABU) shown as mean ± SD, n = 3. Statistically significant differences compared to CMS NT, *p ⩽ 0.05, **p ⩽ 0.01, ***p ⩽ 0.001. (For the interpretation of the references to color in this figure legend, the reader is referred to the web version of this article.)

particles and not drug dissolution or solubilization. Additionally, dendrimers can act as penetration enhancers by interacting with the skin surface lipids and proteins and thus loosening the tightly packed SC structure [42]. Findings which underline this hypothesis have been made by our group using fluorescence lifetime imaging microscopy (FLIM). FLIM revealed intense interactions between CMS nanotransporters and the SC which was not observed in tape stripped skin [18]. Currently, we are evaluating in detail the interactions of polymeric carrier systems with the skin lipids and proteins in order to unravel the mechanism of enhanced drug delivery.

3.3. Biocompatibility and phototoxicity

The toxicity of dendrimers is concentration and generation dependent with higher generations being more toxic as the number of surface groups double with each increasing generation [43]. A decrease in toxicity could be achieved by specific surface modifications. Nevertheless, some functional groups, particularly amines, are important for drug encapsulation and delivery, but also induce toxicity. Hence, there is a need to balance biocompatibility and efficacy. PG–PEG particles are neutral particles – a prerequisite for good biocompatibility.

In order to evaluate the biocompatibility of the PG–PEG particles, we performed the MTT and NRU assay in a first step. We employed the endothelial cells HUVEC because of potential *i.v.* applications and due to the likeliness of systemic absorption when being applied onto damaged or diseased skin. Additionally, we investigated the effects on primary human keratinocytes (NHK) and fibroblasts (NHDF) due to the intended dermal use of the particles. The results of the cytotoxicity assays (MTT test, Fig. 4; and NRU assay, Fig. S1) indicate that the PG–PEG particles are well tolerated by HUVECs, respectively. The metabolic activity was not reduced and no cytotoxic effects were observed even after 48 h.

NHDF showed higher sensitivity indicated by significantly reduced cell viabilities particularly for SK1 (cell viability ⩽80%). This effect was most pronounced after 48 h. In NHK, incubation with SK1 and SK2 (0.05%, respectively) resulted in significantly reduced cell viabilities indicating increased sensitivity. These effects again were most pronounced after 48 h. For all tested formulations and time points, only SK5 gave cell viabilities ⩾80%, respectively, similar to the results with CMS nanotransporters. Nevertheless, using the lower concentration (0.005%) SK1–SK5 consistently showed tolerable biocompatibility, whereas SK3–SK5 showed the best biocompatibilities. Concurrently, the NRU assay

revealed significantly reduced cell viability only for SK1 and SK2 in NHK (0.05%) following 48 h incubation (NHK viability 57% and 40%, respectively). For the other particles and concentrations no cytotoxicity was observed (Fig. S1). As expected, the positive control SDS 0.01% drastically reduced the cell viability by 85% or more in both assays and all tested cell types (Fig. 4).

Our data show that the larger particles (SK1–SK2) were more cytotoxic than the smaller particles (SK3–SK5). This was surprising as cytotoxicity often increases with decreasing particle sizes [44,45]. Nevertheless, one potential explanation is the difference in the synthetic approach and resulting structural differences. Synthesizing SK1 and SK2 via a randomly alkylated approach produced less defined structures with alkyl chains at random positions on terminal and hydroxyl groups of the PG. These alkyl chains may have interacted with the cell membrane due to hydrophobic interactions and disturb the barrier integrity [46]. In contrast, SK3–SK5 just exhibited alkyl substitution in the core and not in terminal regions.

The data from the NRU assay substantiate this hypothesis as reduced cell viability was only observed for SK1 and SK2 in NHK (0.05%) following 48 h incubation (NHK viability 57% and 40%, respectively). Since the alkyl chains were more located on the outside in SK1 and SK2, they could interact with cell membranes.

The biocompatibility of dendritic PG-based particles was investigated systematically by Khandare et al. [47]. Our results are well in line with these findings. One major factor determining the cytotoxicity of particles is their surface charge as shown for PG with higher amine functionality, PAMAM or PEI dendrimers [43,47]. Specifically particles that have amine groups on their surface are expected to be at least partially protonated at a moderate pH, which leads to a positive surface charge. Similar data were reported by the group of Ghandehari who investigated the influence of size, surface charge, and surface functionality of PAMAM on the toxicity in immunocompetent mice. A clear trend was observed based on the surface charge and functional groups of the dendrimers regardless of their size. Amine-terminated dendrimers were fatal at doses >10 mg/kg causing hematological complications, whereas carboxyl- and hydroxyl-terminated dendrimers of similar sizes were tolerated at 50-fold higher doses [48].

Additionally, a phototoxicity test in the Balb/c 3T3 fibroblast cell line was conducted. When applying nanoparticles or formulations onto the skin not only reactivity with the skin but also environmental factors such as UV irradiation are of relevance. Phototoxicity is defined as an inflammatory reaction of the skin
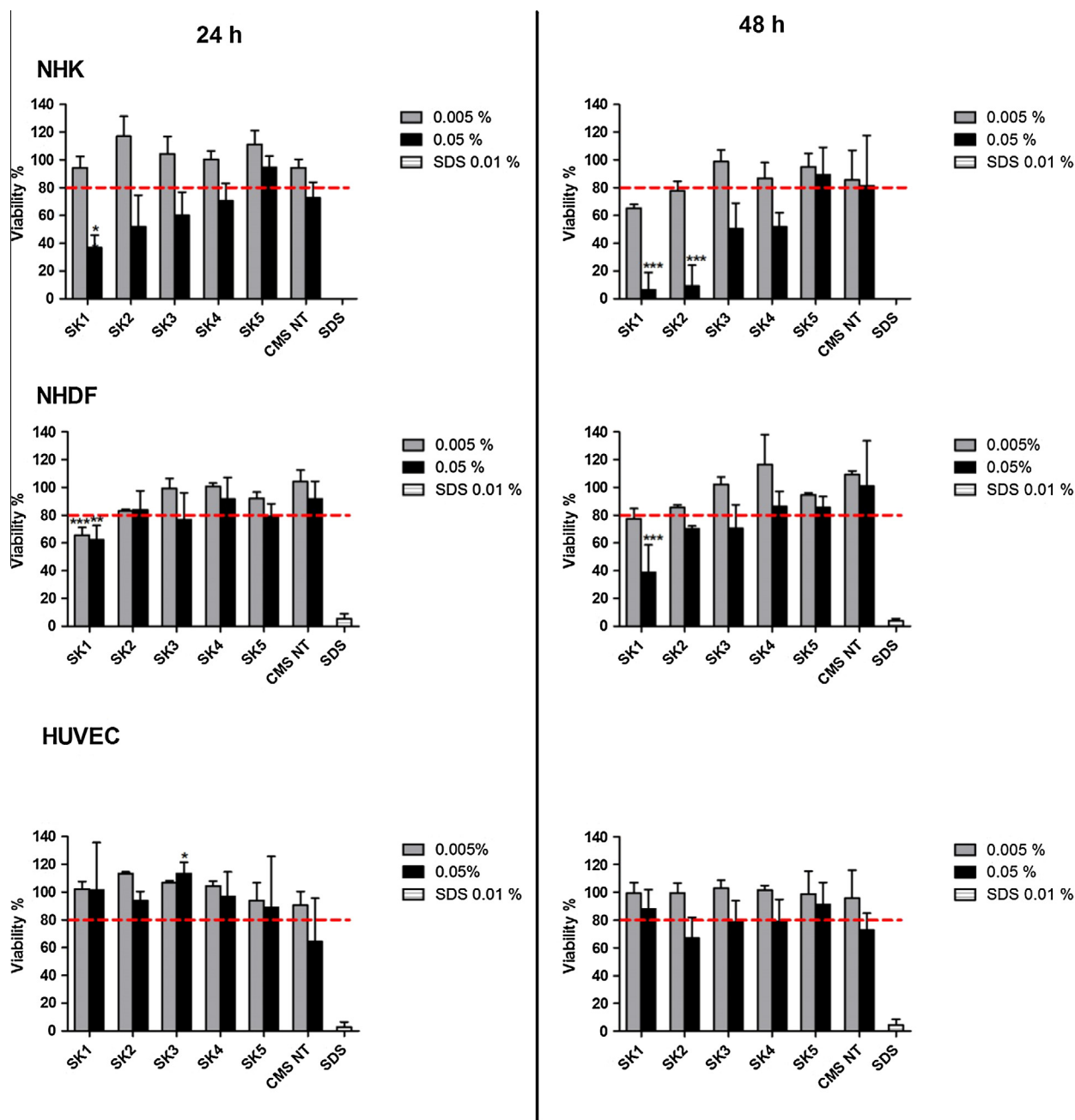
Fig. 4. MTT Assay: Cell viability (mean ± SD; $n = 3$) of human keratinocytes (NHK), fibroblasts (NHDF) and endothelial cells (HUVEC) following the exposure of PG–PEG nanoparticles SK1–SK5 (0.005% gray column; 0.05% black column) or SDS 0.01% (positive control) for 24 and 48 h, respectively. Statistically significant differences compared to CMS NT, $p \leqslant 0.05$, $^{**}p \leqslant 0.01$, $^{***}p \leqslant 0.001$. (For the interpretation of the references to color in this figure legend, the reader is referred to the web version of this article.)

after exposure to a chemical compound and (mainly) UVA irradiation and is characterized by cytotoxicity or the formation of radicals which ultimately react with healthy cells or tissues. Here, we focused on the most efficient particles with respect to dermal drug delivery (SK4 and SK5) and SK1 that exhibited distinct cytotoxicity. A phototoxic potential of the nanoparticles, however, was not observed (PIF not detectable; MPE < 0.1, respectively), whereas UVA-irradiation clearly induced chlorpromazine-mediated phototoxicity (PIF > 5, MPE > 0.15) proving adequate test performance (Table S1).

3.4. Irritation potential

When applying products onto the skin, not only cytotoxic or phototoxic effects are of interest but also irritancies that are

provoked by the respective formulations. Since accidental or intentional exposure of topical formulations to the eyes can result in redness or even severe reactions such as the loss of vision [49], an evaluation of the eye irritation potential is crucial [50]. In order to replace the Draize eye irritation test which is conducted in rabbits and has long been considered as the gold standard, alternative approaches have been developed such as the red blood cell (RBC) test [33] and the HET-CAM test [51] that enable estimations about the irritation potential of the nanoparticles. Both were performed following the respective INVITTOX protocols.

The RBC test is based on the potential of a compound to disrupt cell membranes and thus, to induce hemoglobin leakage from freshly isolated red blood cells. The concentration of the positive control SDS for 50% hemolysis was calculated with 0.0042%. When incubating the PG–PEG nanoparticles with the red blood cells, even
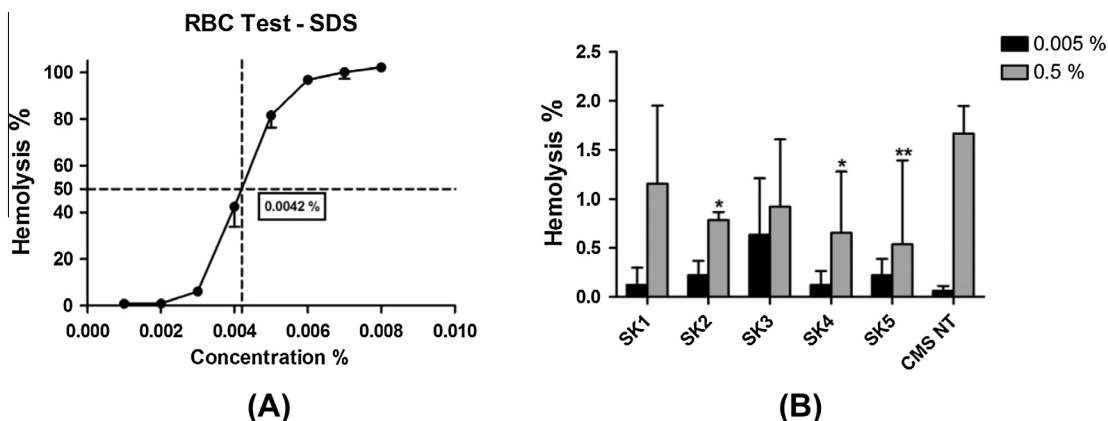
Fig. 5. RBC test: Percentage of hemolysis following exposure to (A) SDS (positive control) and (B) the PG–PEG nanoparticles SK1–SK5 (0.005% gray columns, 0.5% black columns), mean ± SD; n = 4. Statistically significant differences compared to CMS NT, $p \leqslant 0.05$, **$p \leqslant 0.01$.
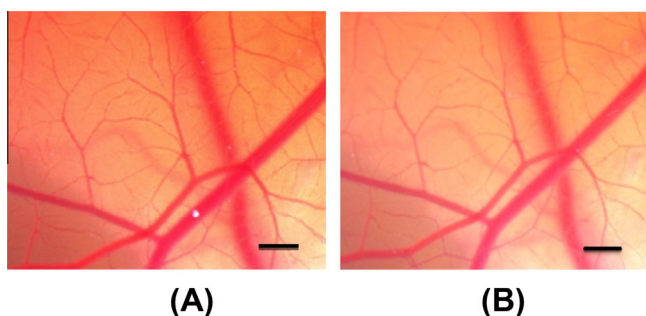
Fig. 6. HET-CAM Test: Representative images of the chorioallantoic membrane before (A) and after application of SK4 nanoparticles (0.05%) for 5 min (B). No signs of irritation (hemorrhage, vessel lysis, or coagulation) were also detected with SK1 and SK5, respectively. The bars refer to 1 mm. (For the interpretation of the references to color in this figure legend, the reader is referred to the web version of this article.)

red blood cells are often associated with other changes in the hematocrit or white blood cells count. However, such effects were not investigated in our study. Nevertheless, the low level of effects in the RBC test suggests minor interactions with other hematological factors.

The results of the RBC test were verified using a second approach. In the HET-CAM test, hemorrhage, lysis, and coagulation of the blood vessels of the chorioallantoic membrane (CAM) were monitored for 5 min. To objectify response evaluation, Texapon ASV, sodium hydrochloride and acetic acid were tested in parallel for reference and allowed a differentiation between none, weak, moderate, and severe reactions. Once more, we focused on SK1, SK4, and SK5 PG–PEG nanoparticles. No changes in the CAM were observed (Fig. 6) which indicated that the PG–PEG nanoparticles were devoid of a major irritant potential. No conclusions could be drawn concerning slight irritations as the HET-CAM test only allows exclusion of major irritations. Nevertheless, the results of both the RBC and HET-CAM tests clearly indicate low irritation potential. Our group has previously reported on the lack of irritancy for CMS nanotransporters [53].

3.5. Genotoxicity

The Comet assay is a common method to assess the genotoxicity of chemicals in various cell types and tissues including skin-derived cells [54,55]. The cells were exposed to PG–PEG SK1 and SK4 (0.05%, 0.005%) for 24 h and 72 h, respectively. The least toxic

100× higher particle concentrations (0.5%) resulted in negligible hemolysis rates of about ⩽2% (Fig. 5).

Once again, good biocompatibility was shown for SK1–SK5 and the CMS nanotransporters, the major reason being the neutral surface charge of the nanoparticles. Free cationic terminal groups of dendrimers interacted with the RBC's membrane and resulted in hemolysis [52]. Several other studies showed hemolysis rates ⩾15% up to 80% for charged dendrimers [43]. Interactions with

Fig. 7. Comet assay: The DNA damage was measured by the tail moment of DNA in keratinocytes (NHK) and fibroblasts (NHDF) after exposure to PG–PEG nanoparticles (SK1, SK4, and SK5) for 24 h (white columns) and 72 h (gray columns). MMS (5 μM) served as positive control. The average baseline damage is less than 1 tail moment, respectively. Mean ± SD, n = 3. Statistically significant differences compared to CMS NT, $p \leqslant 0.05$.

PG–PEG SK5 and the CMS nanotransporters [53] were only tested at the higher concentration (0.05%). Baseline DNA damage was 1 tail moment with NHK and even less with NHDF. The tail moment did not exceed 2 following the nanoparticle exposure (Fig. 7). As expected, the positive control MMS significantly induced DNA breaks, tail moments were detected in 112.5 ± 22.0 keratinocytes and 58.5 ± 11.3 fibroblasts. Genotoxicity of dendritic carrier systems was repeatedly reported. For example, cationic phosphorus-containing dendrimers induced DNA damage in human mononuclear blood cells, A549 human cancer cells, and human gingival fibroblasts [56]. Similar findings were published for poly(propylene imine) dendrimers and again a clear correlation between surface charge and interactions with the DNA was drawn [57]. Dendrimers mainly interact with nucleic acids on the basis of ionic interactions between the negatively charged backbone phosphate groups and positively charged amino groups of the polymer. This can be overcome, for example, by adequate surface modification of the respective polymers or by no surface charge at all such as in CMS nanotransporters or PG–PEG particles.

4. Conclusion

Nanoparticles based on dendritic PG are promising drug delivery systems not only for topical applications. Despite the variety of dendritic PG particles described in the literature there is still a need for new systems and synthesis approaches enabling the design of tailorable particles for efficient drug loading, targeted release, and high delivery efficiency.

The data from our present study indicate that despite the high structural similarity, slight variations in the synthetic approach and the substituents attached to the functional groups may significantly alter the nanoparticle size and formation, the drug loading, and ultimately the drug delivery efficiency. Our data indicate that randomly distributed alkyl chains may interact with the cell membrane of cells via hydrophobic interactions and, hence, induce cytotoxicity and disturbances of barrier integrity.

Nevertheless, it underlines the potential of PG-based nanoparticles for dermal delivery but also highlights the importance of fine tuning of the synthetic approach and the major components of dendritic architectures such as the core or the substituents since both may affect delivery efficiency and local tolerability.

Conflict of interest

The authors state no conflict of interest.

Acknowledgment

Appendix A. Supplementary material

Supplementary data associated with this article can be found, in the online version, at http://dx.doi.org/10.1016/j.ejpb.2014.10.014.

References

[1] M. Gupta, U. Agrawal, S.P. Vyas, Nanocarrier-based topical drug delivery for the treatment of skin diseases, Exp. Opin. Drug Deliv. 9 (2012) 783–804.
[2] C. Pegoraro, S. MacNeil, G. Battaglia, Transdermal drug delivery: from micro to nano, Nanoscale 4 (2012) 1881–1894.
[3] T.W. Prow, J.E. Grice, L.L. Lin, R. Faye, M. Butler, W. Becker, E.M. Wurm, C. Yoong, T.A. Robertson, H.P. Soyer, M.S. Roberts, Nanoparticles and microparticles for skin drug delivery, Adv. Drug Deliv. Rev. 63 (2011) 470–491.
[4] J. Khandare, M. Calderon, N.M. Dagia, R. Haag, Multifunctional dendritic polymers in nanomedicine: opportunities and challenges, Chem. Soc. Rev. 41 (2012) 2824–2848.
[5] S. Mignani, S. El Kazzouli, M. Bousmina, J.P. Majoral, Expand classical drug administration ways by emerging routes using dendrimer drug delivery systems: a concise overview, Adv. Drug Deliv. Rev. 65 (2013) 1316–1330.
[6] R. Haag, F. Kratz, Polymer therapeutics: concepts and applications, Angew. Chem. 45 (2006) 1198–1215.
[7] M. Sun, A. Fan, Z. Wang, Y. Zhao, Dendrimer-mediated drug delivery to the skin, Soft Matter 8 (2012) 4301–4305.
[8] L. Uram, M. Szuster, K. Gargasz, A. Filipowicz, E. Walajtys-Rode, S. Wolowiec, In vitro cytotoxicity of the ternary PAMAM G3-pyridoxal-biotin bioconjugate, Int. J. Nanomed. 8 (2013) 4707–4720.
[9] P. Schilrreff, C. Mundina-Weilenmann, E.L. Romero, M.J. Morilla, Selective cytotoxicity of PAMAM G5 core–PAMAM G2.5 shell tecto-dendrimers on melanoma cells, Int. J. Nanomed. 7 (2012) 4121–4133.
[10] N. Malik, R. Wiwattanapatapee, R. Klopsch, K. Lorenz, H. Frey, J.W. Weener, E.W. Meijer, W. Paulus, R. Duncan, Dendrimers: relationship between structure and biocompatibility in vitro, and preliminary studies on the biodistribution of 125I-labelled polyamidoamine dendrimers in vivo, J. Control. Release 65 (2000) 133–148.
[11] H.T. Chen, M.F. Neerman, A.R. Parrish, E.E. Simanek, Cytotoxicity, hemolysis, and acute in vivo toxicity of dendrimers based on melamine, candidate vehicles for drug delivery, J. Am. Chem. Soc. 126 (2004) 10044–10048.
[12] M. Calderon, M.A. Quadir, S.K. Sharma, R. Haag, Dendritic polyglycerols for biomedical applications, Adv. Mater. 22 (2010) 190–218.
[13] R.K. Kainthan, J. Janzen, E. Levin, D.V. Devine, D.E. Brooks, Biocompatibility testing of branched and linear polyglycidol, Biomacromolecules 7 (2006) 703–709.
[14] A. Chiang, E. Tudela, H.I. Maibach, Percutaneous absorption in diseased skin: an overview, J. Appl. Toxicol.: JAT 32 (2012) 537–563.
[15] V.R. Leite-Silva, M. Le Lamer, W.Y. Sanchez, D.C. Liu, W.H. Sanchez, I. Morrow, D. Martin, H.D. Silva, T.W. Prow, J.E. Grice, M.S. Roberts, The effect of formulation on the penetration of coated and uncoated zinc oxide nanoparticles into the viable epidermis of human skin in vivo, Eur. J. Pharm. Biopharm. 84 (2013) 297–308.
[16] L.L. Lin, J.E. Grice, M.K. Butler, A.V. Zvyagin, W. Becker, T.A. Robertson, H.P. Soyer, M.S. Roberts, T.W. Prow, Time-correlated single photon counting for simultaneous monitoring of zinc oxide nanoparticles and NAD(P)H in intact and barrier-disrupted volunteer skin, Pharm. Res. 28 (2011) 2920–2930.
[17] M.R. Radowski, A. Shukla, H. von Berlepsch, C. Bottcher, G. Pickaert, H. Rehage, R. Haag, Supramolecular aggregates of dendritic multishell architectures as universal nanocarriers, Angew. Chem. 46 (2007) 1265–1269.
[18] N. Alnasif, C. Zoschke, E. Fleige, R. Brodwolf, A. Boreham, E. Ruhl, K.M. Eckl, H.F. Merk, H.C. Hennies, U. Alexiev, R. Haag, S. Küchler, M. Schäfer-Korting, Penetration of normal, damaged and diseased skin – an in vitro study on dendritic core–multishell nanotransporters, J. Control Release 185 (2014) 45–50.
[19] S. Küchler, M.R. Radowski, T. Blaschke, M. Dathe, J. Plendl, R. Haag, M. Schäfer-Korting, K.D. Kramer, Nanoparticles for skin penetration enhancement – a comparison of a dendritic core–multishell-nanotransporter and solid lipid nanoparticles, Eur. J. Pharm. Biopharm. 71 (2009) 243–250.
[20] S. Küchler, M. Adbel-Mottaleb, A. Lamprecht, M.R. Radowski, R. Haag, M. Schäfer-Korting, Influences of nanocarriers' type and size on skin delivery of hydrophilic agents, Int. J. Pharm. 377 (2009) 169–172.
[21] A. Sunder, R. Mulhaupt, R. Haag, H. Frey, Hyperbranched polyether polyols: a modular approach to complex polymer architectures, Adv. Mater. 12 (2000) 235–+.
[22] S. Kumar, A. Mohr, A. Kumar, S.K. Sharma, R. Haag, Synthesis of biodegradable amphiphilic nanocarriers by chemo-enzymatic transformations for the solubilization of hydrophobic compounds, Int. J. Artif. Organs 34 (2011) 84–92.
[23] I. Kurniasih, H. Liang, S. Kumar, A. Mohr, S.K. Sharma, J.P. Rabe, R. Haag, A bifunctional nanocarrier based on amphiphilic hyperbranched polyglycerol derivatives, J. Mater. Chem. B (2013) 3569–3577.
[24] M. Schäfer-Korting, U. Bock, W. Diembeck, H.J. Düsing, A. Gamer, E. Haltner-Ukomadu, C. Hoffmann, M. Kaca, H. Kamp, S. Kersen, M. Kietzmann, H.C. Korting, H.U. Krächter, C.M. Lehr, M. Liebsch, A. Mehling, C. Müller-Goymann, F. Netzlaff, F. Niedorf, M.K. Rübbelke, U. Schafer, C. Schmidt, S. Schreiber, H. Spielmann, A. Vuia, M. Weimer, The use of reconstructed human epidermis for skin absorption testing: results of the validation study, Altern. Lab. Anim. 36 (2008) 161–187.
[25] E. Borenfreund, J.A. Puerner, Toxicity determined in vitro by morphological alterations and neutral red absorption, Toxicol. Lett. 24 (1985) 119–124.
[26] G. Repetto, A. del Peso, J.L. Zurita, Neutral red uptake assay for the estimation of cell viability/cytotoxicity, Nat. Protoc. 3 (2008) 1125–1131.
[27] ECVAM, INVITOX Protocol n° 78 3T3 NRU phototoxicity assay, in: In vitro tests protocols, 2004.
[28] M. Liebsch, H. Spielmann, INVITTOX Protocol No. 78: 3T3 NRU Phototoxicity Assay, European Commission DG-JRC, ECVAM, SIS Database, 1998 (Last update December 2008).
[29] H.-G. Holzhütter, A general measure of in vitro phototoxicity derived from pairs of dose response curves and its use for predicting the in vivo phototoxicity of chemicals, ATLA 25 (1997) 445–462.
[30] B. Peters, H.-G. Holzhütter, In vitro phototoxicity testing: development and validation of a new concentration response analysis software and biostatistical

analyses related to the use of various prediction models, Altern. Lab. Anim. 30 (2002) 415–432.

[31] ECVAM, INVITTOX Protocol n° 96 Heńs Egg Test on the Chorioallantoic Membrane (HET-CAM), In vitro tests protocols, <http://ecvam-dbalm.jrc. ec.europa.eu/>, 2007.

[32] ECVAM, INVITTOX Protocol number 37, Red blood cell test system, in: In vitro tests protocols, 1992.

[33] W.J. Pape, U. Hoppe, Standardization of an in vitro red blood cell test for evaluating the acute cytotoxic potential of tensides, Arzneimittelforschung 40 (1990) 498–502.

[34] N.P. Singh, M.T. McCoy, R.R. Tice, E.L. Schneider, A simple technique for quantitation of low levels of DNA damage in individual cells, Exp. Cell Res. 175 (1988) 184–191.

[35] W. Diembeck, H. Beck, F. Benech-Kieffer, P. Courtellemont, J. Dupuis, W. Lovell, M. Paye, J. Spengler, W. Steiling, Test guidelines for in vitro assessment of dermal absorption and percutaneous penetration of cosmetic ingredients. European Cosmetic, Toiletry and Perfumery Association, Food Chem. Toxicol. 37 (1999) 191–205.

[36] A. Boreham, M. Pfaff, E. Fleige, R. Haag, U. Alexiev, Nanodynamics of dendritic core–multishell nanocarriers, Langmuir: ACS J. Surf. Colloids 30 (2014) 1686–1695.

[37] M.M. Abdel-Mottaleb, B. Moulari, A. Beduneau, Y. Pellequer, A. Lamprecht, Nanoparticles enhance therapeutic outcome in inflamed skin therapy, Eur. J. Pharm. Biopharm. 82 (2012) 151–157.

[38] C.S. Campbell, L.R. Contreras-Rojas, M.B. Delgado-Charro, R.H. Guy, Objective assessment of nanoparticle disposition in mammalian skin after topical exposure, J. Control. Release 162 (2012) 201–207.

[39] T. Gratieri, U.F. Schaefer, L. Jing, M. Gao, K.H. Kostka, R.F. Lopez, M. Schneider, Penetration of quantum dot particles through human skin, J. Biomed. Nanotechnol. 6 (2010) 586–595.

[40] F.F. Larese, F. D'Agostin, M. Crosera, G. Adami, N. Renzi, M. Bovenzi, G. Maina, Human skin penetration of silver nanoparticles through intact and damaged skin, Toxicology 255 (2009) 33–37.

[41] B. Baroli, Penetration of nanoparticles and nanomaterials in the skin: fiction or reality?, J Pharm. Sci. 99 (2010) 21–50.

[42] V.V. Venuganti, O.P. Perumal, Poly(amidoamine) dendrimers as skin penetration enhancers: influence of charge, generation, and concentration, J. Pharm. Sci. 98 (2009) 2345–2356.

[43] K. Jain, P. Kesharwani, U. Gupta, N.K. Jain, Dendrimer toxicity: let's meet the challenge, Int. J. Pharm. 394 (2010) 122–142.

[44] J. Ai, E. Biazar, M. Jafarpour, M. Montazeri, A. Majdi, S. Aminifard, M. Zafari, H.R. Akbari, H.G. Rad, Nanotoxicology and nanoparticle safety in biomedical designs, Int. J. Nanomed. 6 (2011) 1117–1127.

[45] A. Elsaesser, C.V. Howard, Toxicology of nanoparticles, Adv. Drug Deliv. Rev. 64 (2012) 129–137.

[46] O. Inui, Y. Teramura, H. Iwata, Retention dynamics of amphiphilic polymers PEG-lipids and PVA-alkyl on the cell surface, ACS Appl. Mater. Interfaces 2 (2010) 1514–1520.

[47] J. Khandare, A. Mohr, M. Calderon, P. Welker, K. Licha, R. Haag, Structure–biocompatibility relationship of dendritic polyglycerol derivatives, Biomaterials 31 (2010) 4268–4277.

[48] K. Greish, G. Thiagarajan, H. Herd, R. Price, H. Bauer, D. Hubbard, A. Burckle, S. Sadekar, T. Yu, A. Anwar, A. Ray, H. Ghandehari, Size and surface charge significantly influence the toxicity of silica and dendritic nanoparticles, Nanotoxicology 6 (2012) 713–723.

[49] M.P. Vinardell, M. Mitjans, Alternative methods for eye and skin irritation tests: an overview, J. Pharm. Sci. 97 (2008) 46–59.

[50] C. Eskes, S. Bessou, L. Bruner, R. Curren, J. Harbell, P. Jones, R. Kreiling, M. Liebsch, P. McNamee, W. Pape, M.K. Prinsen, T. Seidle, P. Vanparys, A. Worth, V. Zuang, Eye irritation, Altern. Lab. Anim. 33 (Suppl. 1) (2005) 47–81.

[51] W. Steiling, M. Bracher, P. Courtellemont, O. de Silva, The HET-CAM, a useful in vitro assay for assessing the eye irritation properties of cosmetic formulations and ingredients, Toxicol. In Vitro 13 (1999) 375–384.

[52] D. Bhadra, S. Bhadra, S. Jain, N.K. Jain, A PEGylated dendritic nanoparticulate carrier of fluorouracil, Int. J. Pharm. 257 (2003) 111–124.

[53] N.B. Wolf, S. Küchler, M.R. Radowski, T. Blaschke, K.D. Kramer, G. Weindl, B. Kleuser, R. Haag, M. Schäfer-Korting, Influences of opioids and nanoparticles on in vitro wound healing models, Eur. J. Pharm. Biopharm. 73 (2009) 34–42.

[54] E. Rojas, M.C. Lopez, M. Valverde, Single cell gel electrophoresis assay: methodology and applications, J. Chromatogr. B Biomed. Sci. Appl. 722 (1999) 225–254.

[55] T.Y. Tzung, T.M. Runger, Assessment of DNA damage induced by broadband and narrowband UVB in cultured lymphoblasts and keratinocytes using the comet assay, Photochem. Photobiol. 67 (1998) 647–650.

[56] P. Gomulak, B. Klajnert, M. Bryszewska, J.P. Majoral, A.M. Caminade, J. Blasiak, Cytotoxicity and genotoxicity of cationic phosphorus-containing dendrimers, Curr. Med. Chem. 19 (2012) 6233–6240.

[57] B. Ziemba, G. Matuszko, D. Appelhans, B. Voit, M. Bryszewska, B. Klajnert, Genotoxicity of poly(propylene imine) dendrimers, Biopolymers 97 (2012) 642–648.